The sequestration efficiency of the deep ocean

Benoît Pasquier[1,2], Richard J. Matear[3], Matthew A. Chamberlain[3], Tilo Ziehn[4], David K. Hutchinson[5], François W. Primeau[6], Yi Liu[7], and Ann Bardin[6]

[1]Independent Researcher
[2]School of Mathematics and Statistics, University of New South Wales, Sydney, Australia
[3]Commonwealth Scientific and Industrial Research Organisation, Hobart, Australia
[4]Commonwealth Scientific and Industrial Research Organisation, Aspendale, Australia
[5]Climate Change Research Centre, School of Biological, Earth and Environmental Sciences, University of New South Wales, Sydney, NSW, Australia
[6]Department of Earth System Science, University of California, Irvine, Irvine, USA
[7]Department of Geosciences, High Meadows Environmental Institute, Princeton University, Princeton, USA

Key Points:

- We introduce an idealized but computationally efficient method to estimate transit time distributions (TTDs) from climate-model archives
- In ACCESS-ESM1.5 it takes up to 1300 ± 350 years for $10\,\%$ of the water on the North Pacific seabed to reach the ocean surface
- Under future SSP3-7.0 climate change the slower ocean circulation lengthens transit times by $\sim 30\,\%$ which exceeds $\sim 20\,\%$ climate variability

Corresponding author: BP, `b.pasquier@unsw.edu.au`

Corresponding author: RJM, `richard.matear@csiro.au`

Abstract

Ocean sediments may provide adequate long-term storage for carbon dioxide removal (CDR), with the abyssal ocean providing extra sequestration. The transit of carbon from seafloor release to ocean surface can take up to millennia, as it occurs through many pathways characterized by long-tailed transit-time distributions (TTDs). Here, we introduce an idealized methodological framework for efficiently computing these TTDs from climate-model archives. We apply this framework to one Earth System Model and estimate the deep ocean sequestration efficiency for the 2030s and 2090s ocean circulations. We find the highest sequestration efficiencies on abyssal plains isolated from the deep branches of the conveyor belt, such as the North Pacific Basins, where less than 10 % of water makes contact with the surface after 1000 years. The climate-warming induced slowdown of the 2090s deep ocean circulation extends return times by about 30 %, which exceeds internal variability ($\sim 20\,\%$) estimated from the ensemble of simulations.

Plain Language Summary

To limit global warming to 2 °C we must actively remove CO_2 from the atmosphere. A good place for storing this removed carbon may be the sediments of the deep ocean, in part because the ocean provides an extra layer of sequestration. Carbon can travel through many ocean pathways from the seafloor to the surface, and this transit can take up to millennia. The transit times associated with this transport can be expensive to simulate with a climate model, even on powerful computers. Here, we introduce an approximate but highly efficient method to reproduce these simulations based on climate-model archives only, i.e., without running the climate models themselves. Applying this method, we identify preferred locations for sedimentary storage such as the North Pacific Basins, where less than 10 % of carbon will return to the surface after 1000 years. We also find that climate change weakens the deep ocean circulation and tends to extend sequestration by about 30 % by 2100.

1 Introduction

As greenhouse gas emissions into the atmosphere continue to rise, limiting global warming to less than 2 °C cannot be achieved by only reducing carbon dioxide (CO_2) emissions: Carbon Dioxide Removal (CDR) technology will be required (e.g., Gattuso et al., 2021; Riahi et al., 2023). The ocean is potentially a good candidate for carbon storage (Doney et al., 2024), currently holding about 50 times more carbon than the atmosphere (DeVries, 2022). And while the ocean has absorbed about 25% of anthropogenic CO_2 and will naturally absorb more in the future, this process is slow relative to the pace of climate change (Wong & Matear, 1998).

Many different marine-based CDR (mCDR) strategies have been proposed, including fertilizing the ocean (Pessarrodona et al., 2023), growing seaweed (Hurd et al., 2022; DeAngelo et al., 2023; Ross et al., 2023), artificial upwelling or downwelling (Oschlies et al., 2010), increasing alkalinity (Lenton et al., 2018), and injecting carbon into the sediments (Herzog, 2001; Ringrose, 2020). Key to effective mCDR is the carbon sequestration time, i.e., the time that the removed carbon is sequestered before being released back into the atmosphere (e.g., Siegel et al., 2021). This sequestration time is tightly linked to the time that water takes to return to the ocean surface where carbon can be exchanged with the atmosphere.

This water return time has been estimated in a number of contexts using various models and configurations (e.g., Holzer & Hall, 2000; Primeau, 2005; Primeau & Holzer, 2006; Haine et al., 2008; DeVries & Primeau, 2011; DeVries et al., 2012; DeVries & Holzer, 2019; Holzer et al., 2020, 2021; Siegel et al., 2021; Pasquier, Holzer, & Chamberlain, 2024; Nowicki et al., 2024; Haine et al., 2024). Yet, the effect of climate change and climate variability on the return time have not been investigated. This is likely because it is difficult to directly simulate in most ocean models. While it is easy to log the return times of a dye injected in the ocean interior, it may require thousands of years of simulation time (Primeau, 2005), and doing so for many injection locations quickly becomes computationally prohibitive. A state-of-the-art, computationally efficient workaround is to track water backwards in time instead, i.e., from the surface back into the ocean interior, using what is called an adjoint boundary propagator (e.g., Holzer & Hall, 2000; Primeau, 2005; Haine et al., 2024).

Here, we focus on the ocean pathways that start from the seafloor and return to the surface to quantify the sequestration efficiency of the deep ocean for carbon storage. In reality, carbon would likely be stored in the sediments with the ocean providing an additional layer of sequestration delaying the return of carbon back into the atmosphere. This study specifically addresses the following questions:

1. How long does it take for water at the seabed to return to the ocean surface?
2. What fraction of water remains out of contact with the atmosphere after a given time (e.g., 1000 years)?
3. How do climate variability and climate change affect the return time from seabed to surface?

To answer these questions, we compute the transit-time distribution (TTD) for water to transit from the seabed to the surface layer using monthly ocean transport matrices built from archives of the Australian Community Climate and Earth-System Simulator (ACCESS-ESM1.5; Ziehn et al., 2020). The TTD is efficiently computed from an adjoint boundary propagator for the seasonally varying annually periodic flow representing the ocean circulation climatology of the 2030s for the Shared Socioeconomic Pathway SSP3-7.0 (Riahi et al., 2017; Arias et al., 2021). We assess the effect of climate change by the end of the century by repeating the TTD computation for the 2090s. The effect of climate variability is assessed using the 40-member ensemble of realizations of ACCESS-ESM1.5 submitted to the 6th phase of the Climate Model Intercomparison Project (CMIP6).

2 Methods

Our simulations are conducted in the idealized context of perpetually repeating a seasonally varying but annually periodic year representing the ocean circulation climatology of a given period. This idealized framework has multiple advantages. Chiefly, it allows us to simulate tracers for thousands of years, well beyond the available 1850–2100 window of CMIP6 archives. In addition, it avoids the complications from model drift and simplifies the mathematics while retaining the features of seasonality (as opposed to the steady-state context of Holzer et al., 2020; Pasquier, Holzer, & Chamberlain, 2024; Pasquier, Holzer, Chamberlain, Matear, & Bindoff, 2024). This facilitates computing the adjoint boundary propagator required for computing the sequestration efficiency. Furthermore, it affords us considerable computational savings, with wall times about 150× shorter than standard climate-model simulations.

2.1 Ocean Transport Matrices

We build matrices from climate-model archives following Chamberlain et al. (2019) but improve on their approach by capturing seasonality. For a given period (e.g., the 2030s) we build 12 monthly transport matrices $\mathbf{T}_m$, such that $\mathbf{T}_1$ represents the January climatology of the circulation, $\mathbf{T}_2$ represents February, and so on. Each transport matrix $\mathbf{T}_m$ is a discretization of the climatological mean advective–eddy-diffusive transport operator $\mathcal{T} \equiv \boldsymbol{u} \cdot \nabla - \nabla \cdot \mathbf{K} \nabla$ for that month, where $\boldsymbol{u}$ is the resolved and parameterized advective velocity, and $\mathbf{K}$ is the parameterized diffusivity tensor. Multiplying the transport matrix $\mathbf{T}_m$ by a tracer concentration vector $\boldsymbol{c}$ is the discrete equivalent of multiplying the transport operator $\mathcal{T}$ by the corresponding concentration field c and gives the divergence of the advective–eddy-diffusive flux of the tracer.

Our transport matrices are built from ACCESS-ESM1.5 archives (Ziehn et al., 2020). Its ocean component is the Modular Ocean Model version 5 (MOM5 Griffies, 2012). MOM5 is configured with a nominal horizontal resolution of $1^\circ \times 1^\circ$ and 50 vertical levels with cell thicknesses ranging from 10 m at the surface to 335 m for the deepest level. The MOM5 grid is tripolar, with two poles in the Northern Hemisphere located on land.

The resolved horizontal advective fluxes are taken from CMIP6-archived mass-transport variables, and the unresolved Gent–McWilliams and submesoscale advection from CSIRO-archived variables (details in Open Research Section). The vertical advective fluxes are built through mass conservation from the seafloor up and their flux-divergence operator is built using a simple first-order centered scheme. This also improves the method of Chamberlain et al. (2019) by reducing the severe diffusivity of their upwind scheme.

Diffusion is parameterized as a simple first-order scheme with global diffusivity constants that are calibrated against the ACCESS-ESM1.5 water age. Specifically, we apply constant background horizontal diffusivity $\kappa_\mathrm{H} = 300\,\mathrm{m}^2\,\mathrm{s}^{-1}$ and vertical diffusivity $\kappa_\mathrm{V} = 3 \times 10^{-5}\,\mathrm{m}^2\,\mathrm{s}^{-1}$, with additional vertical diffusion in the mixed layer ($\kappa_\mathrm{VML} = 1\,\mathrm{m}^2\,\mathrm{s}^{-1}$). These constants are calibrated for our transport-matrix estimate of the water age to match the online ACCESS-ESM1.5 1850s age. Since the CMIP6 archived ACCESS-ESM1.5 age was not fully spun up (Mannis et al., 2024), we used Anderson Acceleration (Khatiwala, 2023, 2024) to spin it up efficiently ourselves.

2.2 Sequestration Efficiency and Transit Time

The key metric herein is the sequestration efficiency, $\mathcal{E}(\boldsymbol{r}, t, \tau)$, which is the fraction of water at location $\boldsymbol{r}$ and time t that will not have reemerged into the surface layer after a time τ (DeVries et al., 2012). The sequestration efficiency is derived from the TTD, which quantifies the probability of all the possible times for water to transit to the surface. Below, we briefly outline the mathematics and computational methodology employed, with details provided in Sections S1 and S2.

The probability density function of the TTD is given by $\tau \mapsto \mathcal{G}^\dagger(\boldsymbol{r}, t, t+\tau)$, where $\mathcal{G}^\dagger$ is a Green function —the adjoint boundary propagator— which we use to track water backwards in time from future surface injection (see Section S1 for details). The sequestration efficiency is given by the complement of the cumulative distribution function of the TTD:

$$\mathcal{E}(\boldsymbol{r}, t, \tau) = \int_\tau^\infty dt'\, \mathcal{G}^\dagger(\boldsymbol{r}, t, t+t'). \tag{1}$$

For simplicity, we average the sequestration efficiency and the timescales discussed throughout over one year. For instance, we consider the mean sequestration efficiency, given by

$$\overline{\mathcal{E}}(\boldsymbol{r}, \tau) \equiv \frac{1}{1\,\mathrm{yr}} \int_{t_\mathrm{i}}^{t_\mathrm{i}+1\,\mathrm{yr}} dt\, \mathcal{E}(\boldsymbol{r}, t, \tau), \tag{2}$$

which is independent of the initial time t_i for annually periodic flow. (Throughout, an overline denotes the mean over one year.) The advantage of this averaging is that it removes the need to carefully stitch back together adjoint simulations (Fig. S1). In practice, $\mathcal{G}^\dagger(\boldsymbol{r}, t_\mathrm{f}-\tau, t_\mathrm{f})$ is computed backwards in time from surface injection at final time t_f as a boundary impulse response (BIR; Eqs. (S4–S5)), and such BIRs are not necessarily TTDs for unsteady flow (see, e.g., Haine et al., 2024). However, averaged over one year of periodic flow, BIR and TTD are identical, and the mean adjoint boundary propagator,

$$\overline{\mathcal{G}^\dagger}(\boldsymbol{r}, \tau) \equiv \frac{1}{1\,\mathrm{yr}} \int_{t_\mathrm{i}}^{t_\mathrm{i}+1\,\mathrm{yr}} dt\, \mathcal{G}^\dagger(\boldsymbol{r}, t, t+\tau), \tag{3}$$

can be directly used to compute the mean sequestration efficiency, which is then simply given by

$$\overline{\mathcal{E}}(\boldsymbol{r}, \tau) = \int_\tau^\infty dt\, \overline{\mathcal{G}^\dagger}(\boldsymbol{r}, t). \tag{4}$$

To put sequestration timescales into context, we also consider the mean transit time, $\Gamma^\dagger(\boldsymbol{r}, t)$, which is the average time for water at $(\boldsymbol{r}, t)$ to reemerge into the surface layer. In theory, its mean $\overline{\Gamma^\dagger}$ can be computed as the 1st moment of the mean TTD as

$$\overline{\Gamma^\dagger}(\boldsymbol{r}) \equiv \int_0^\infty d\tau\, \tau\, \overline{\mathcal{G}^\dagger}(\boldsymbol{r}, \tau). \tag{5}$$

However, a useful property of $\Gamma^\dagger$ in periodic flow is that it obeys a nonlinear equation that we directly solve with a Newton–Krylov method (Bardin et al., 2014), which is considerably more efficient than time stepping $\overline{\mathcal{G}^\dagger}$ over the full TTD (details in Section S2).

3 Results

3.1 Sequestration Efficiency, $\overline{\mathcal{E}}$

Carbon released on the continental shelf quickly returns to the atmosphere, with more than 90 % reaching the surface layer in less than 100 years ($\overline{\mathcal{E}} \leq 10\,\%$; Fig. 1a). In contrast, on the abyssal plain away from the continental shelf, over 90 % of the water has not reached the surface even after 100 years. For longer horizons, more water makes contact with the surface (Fig. 1b,c). By 1000 years, $\overline{\mathcal{E}}$ declines below 90 % everywhere except in the North Pacific Basins.

The patterns of $\overline{\mathcal{E}}$ have the markings of the ocean circulation. The isolated abyssal waters of the North Pacific Basins provide the strongest sequestration efficiencies because these waters sit at the advective terminus of the great ocean conveyor and their return pathways are dominated by slow eddy-diffusion (Holzer & Primeau, 2006; Holzer et al., 2021). Similarly, the Southwest Pacific Basin, north of the Pacific Antarctic Ridge and west of the East Pacific Rise, and the Canary Basin and the North American Basin, east and west of the Mid-Atlantic Ridge, also provide relatively strong sequestration potential. Other basins provide less efficient sequestration, with the least efficient locations near the Southern Ocean (30–90 % after 300 years, 10–50 % after 1000 years), including the Weddell Sea, the Bellingshausen, and the Australian-Antarctic Basins south of the Southeast Indian Ridge, as well as the Crozet Basin, because connections into deep branches of the Antarctic Circumpolar Current (ACC) provide a conduit back to the surface (Toggweiler et al., 2019). Climate variability, quantified here by the 40-member ensemble range, is generally less than 20 % ($\overline{\mathcal{E}}$ units). However, variability in the Weddell Sea is high, ($> 60\,\%$ after 100 years and $\sim 30\,\%$ after 1000 years), likely because of variability in deep water formation and mixed layer depths. For long time horizons ($\tau = 1000$ years), we also find 20–40 % variability in the North American Basin, likely owing to variability in Atlantic Meridional Overturning Circulation (AMOC) and North Atlantic Deep Water (NADW) formation, which can vary strongly across simulations of the same model (e.g., Romanou et al., 2023).

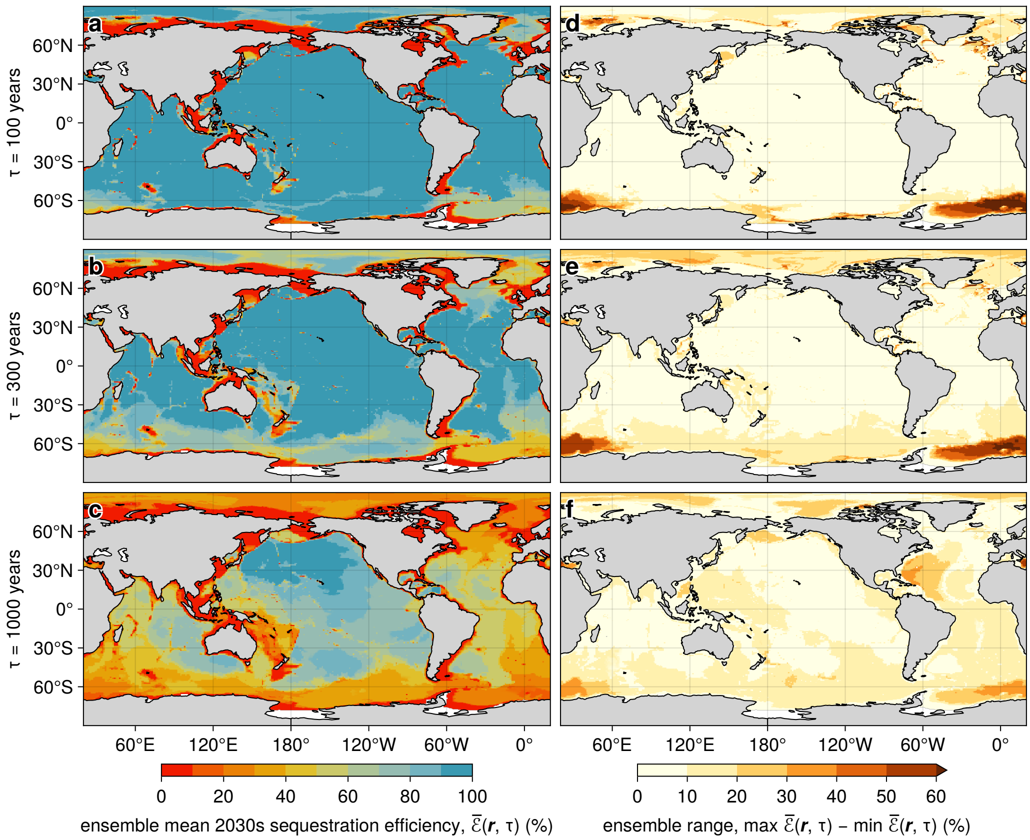

Figure 1. (a–c) Mean sequestration efficiency, $\overline{\mathcal{E}}(\boldsymbol{r}, \tau)$, for seabed water after (a) $\tau = 100$ years, (b) $\tau = 300$ years, and (c) $\tau = 1000$ years, averaged over the 40-member ensemble, for the 2030s circulation. (d–f) Climate variability of (a–c) as quantified by the ensemble $\overline{\mathcal{E}}(\boldsymbol{r}, \tau)$ range, i.e., the ensemble maximum minus the ensemble minimum.

3.2 Characteristic Seafloor-to-Reemergence Timescales

We quantify the ocean's sequestration potential in terms of characteristic timescales of the TTD. To put these timescales in perspective, we start with the mean time to reemergence, $\overline{\Gamma^\dagger}$ (Fig. 2a). On the abyssal plain (below 3000 m), $\overline{\Gamma^\dagger}$ ranges from about 300 to 3000 years. Waters of the Weddell Sea, Australian Antarctic, and Bellingshausen Basins reemerge relatively fast through ACC connections (300–1200 years). Similarly, a fraction of waters of the Arabian Basin and the Somali Abyssal Plain upwell adiabatically into Indian Deep Water (IDW) that returns to the upper ocean (Talley, 2015). Consistent with high $\overline{\mathcal{E}}$, the longest abyssal seafloor-to-reemergence times (more than 3000 years) are found in the North Pacific Basins. We emphasize that our results are specific to ACCESS-ESM1.5, which has a relatively weak deep ocean circulation and is thus expected to overestimate transit times (see Section S3).

Further, we derive the quantiles of the TTD. That is, instead of charting the fraction $\overline{\mathcal{E}}$ of water that remains sequestered for a given time τ, we chart the time that a given fraction of water takes to reemerge (i.e., the time τ for a given value of $\overline{\mathcal{E}}$). For simplicity, we only consider the median ($\overline{\mathcal{E}} = 50\,\%$) and the 10th percentile ($\overline{\mathcal{E}} = 90\,\%$), i.e., the time for half and 10 % of the water to reemerge, respectively (Fig. 2b,c). While their patterns are similar, the median time to reemergence is roughly $30 \pm 15\,\%$ shorter than the mean time to reemergence over the abyssal plain. This is because of ocean mixing, which imparts long tails and strongly skews the TTDs to the right (Primeau & Holzer, 2006; Waugh et al., 2006). The 10th percentile time follows similar geographical patterns and is naturally smaller with significant variations over the abyssal plain. That is, it may take a couple of centuries for 10 % of the water located in the Southern Ocean abyss to reemerge, but it takes more than a millennium for water in the North Pacific Basins.

As we did for the sequestration efficiency, we assess the effect of internal-model climate variability on reemergence timescales by looking at the ensemble range (Fig. 2d–f). We find that $\overline{\Gamma^\dagger}$ varies by 200–400 years or about 15–30 % of the ensemble mean over most of the global abyssal plain. The largest relative internal variability on the abyssal plain is found in the Weddell Sea Basin, where the ensemble range is larger than the ensemble mean. This is consistent with large climate variability in deep water formation and mixed layer depth in the region. Climate variability for the median time to reemergence is similar to the mean time but noticeably smaller in the Weddell Sea. For the smaller

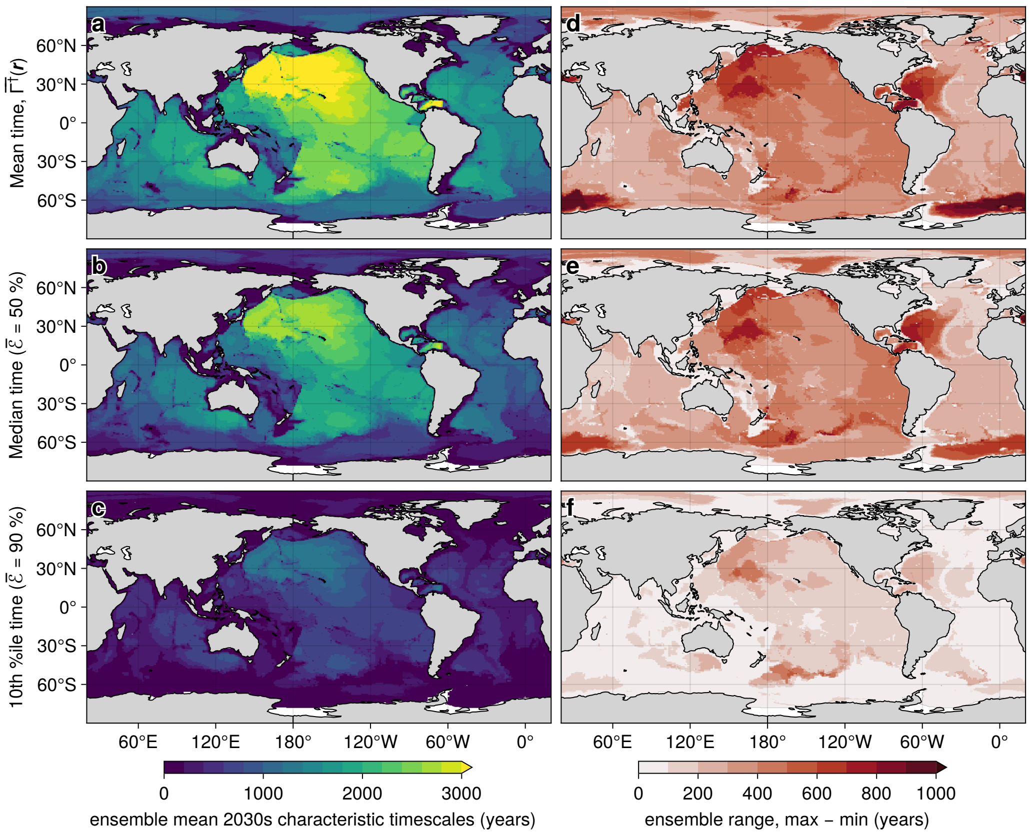

Figure 2. (a) Ensemble mean of the mean time to reemergence, $\overline{\Gamma^{\dagger}}$, at the seafloor, for the 2030s circulation. (b) As (a) but for the median time, i.e., the time for half of the water to reemerge ($\overline{\mathcal{E}} = 50\,\%$). (c) As (b) but for the time for $10\,\%$ of the water to make contact with the surface ($\overline{\mathcal{E}} = 90\,\%$). (d–f) Climate variability of (a–c) as quantified by the ensemble range, i.e., the ensemble maximum minus the ensemble minimum.

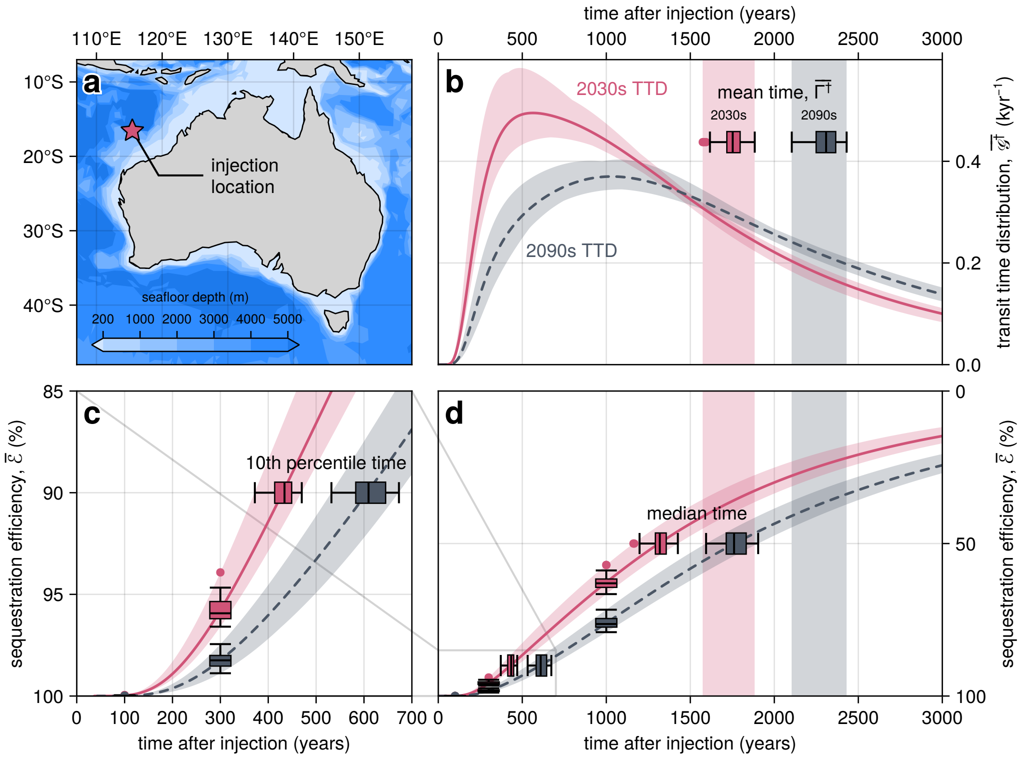

Figure 3. (a) Seafloor injection location (4200 m depth). (b) Ensemble mean (solid lines) and ensemble range (ribbons) of the TTDs for the 2030s (pink) and 2090s (gray), computed as $\overline{\mathcal{G}^{\dagger}}$. The ensemble interquartile ranges of $\overline{\Gamma^{\dagger}}$ are represented as box plots and ensemble ranges as vertical bands. (c) As (b) but for $\overline{\mathcal{E}}$. Ensemble interquartile ranges are shown for the 10th percentile time, the median time, and $\overline{\mathcal{E}}(\tau)$ for $\tau = 100$, 300, and 1000 years. (d) As (c) but zoomed out to 3000 years.

10th percentile time, climate variability in the Weddell Sea is almost entirely subdued (< 100 years) because it takes less than 100 years for 10 % of the Weddell Sea Basin water to reemerge across the 40 members.

3.3 Case Study: Injection on the Argo Abyssal Plain

As a case study, we consider the time series of sequestration for water starting 4200 m deep on the seabed off Northwest Australia (roughly 115.5°E, 16.6°S; Fig. 3a). We chose this location for its proximity to an existing offshore well, but emphasize that these time series are readily available at every ocean location within our framework, making it a useful planning tool for assessing the effectiveness of seabed carbon injection.

The TTD (Fig. 3b) skews strongly to the right, with a mode at about 500–700 years and a long tail extending well beyond our 3000 years of simulation, which is typical for TTDs in the ocean (Primeau & Holzer, 2006; Waugh et al., 2006). At about 1600–1900 years, the mean time to reemergence $\overline{\Gamma^\dagger}$ is more than twice as large as the mode.

Almost no water reemerges into the surface layer in the first 150 years (Fig. 3c,d). About 95 % remains sequestered after 300 years, and 65 % after 1000 years. In terms of characteristic timescales, it takes roughly 400 years for 10 % of the water to reemerge. Owing to the TTD skewness, the median time to reemergence ($\overline{\mathcal{E}} = 50\,\%$), is about 15 % shorter than the mean time to reemergence, $\overline{\Gamma^\dagger}$. That is, it takes about 1300 years for 50 % of the water to reemerge. This suggests that our choice of location is a good candidate for seabed carbon injection as the ocean would provide long-term sequestration in the case of carbon leaking from the sediments.

3.4 Effect From Climate Change

Ventilation is expected to generally decrease with global warming, although the complex reorganization of the global circulation may produce counterintuitive increases (Gnanadesikan et al., 2007; Liu & Primeau, 2023). To investigate the effect of climate change on TTDs and seafloor sequestration efficiency, we repeat our analysis but for the 2090s instead of the 2030s, the expected response being a general increase in sequestration efficiency and return timescales. While our idealized periodic simulations cannot accurately predict a transient future, we emphasize that our 2030s and 2090s simulations provide reasonable bounds for what we might expect from a transient ACCESS-ESM1.5 simulation.

For $\tau = 1000$ and 300 years (Figs. 4, S6), we find $\overline{\mathcal{E}}$ increases by more than 30 % in the Weddell Sea Basin and the Arctic, and by 10–20 % in the Atlantic. Contrastingly, we find mild decreases in the Southwest Pacific Basin north of the Pacific Antarctic Ridge, which possibly indicates emerging connections to deep branches of the ACC caused by a reorganization of the deep ocean circulation. For the short time horizon ($\tau = 100$ years; Fig. S6), the climate-change driven increase in $\overline{\mathcal{E}}$ is generally small (less than +10 %) as it was already large in the 2030s, except in the Weddell Sea (+40 %).

Along with sequestration efficiency, the time to reemergence generally increases by 15–40 % for the climate-change affected 2090s ocean circulation (Figs. 3–4, S6). The largest increases for the mean and median time to reemergence are found in the Weddell Sea

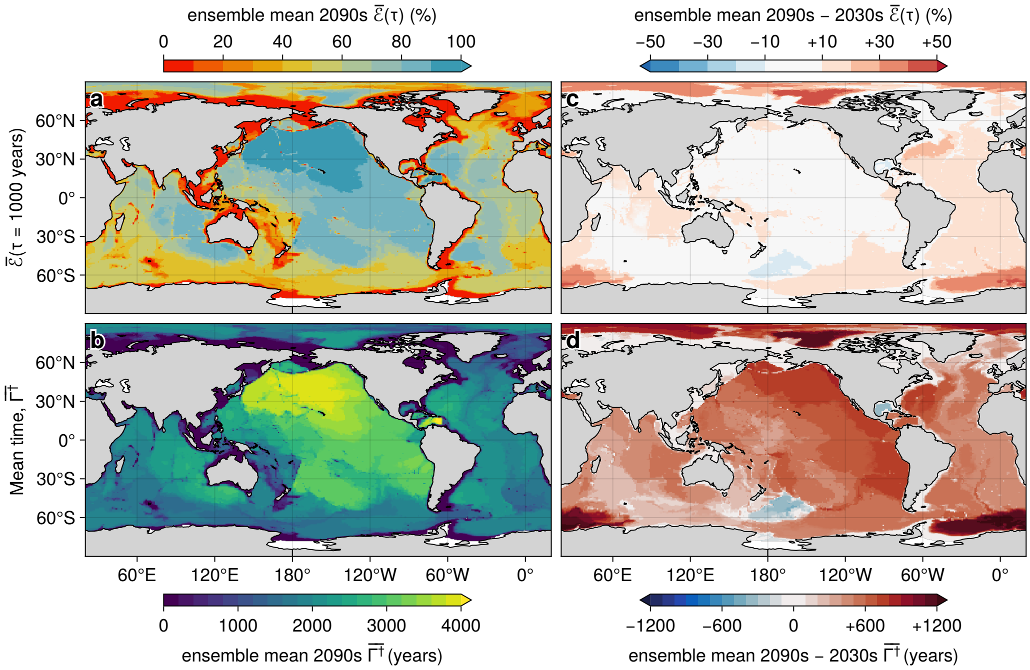

Figure 4. (a,b) As Figs. 1a and 2a but for the 2090s. (c,d) Climate-change effect as quantified by the difference between the ensemble mean 2090s and 2030s.

Basin and in the Arctic (+1000–1200 years), in the Northeast Pacific Basin (+700–800 years), and in the Northwest Atlantic Basin (+600–700 years). The increase in the median and 10th percentile times are smaller in magnitude but remain large relative to their 2030s values (+10–50 %). We note that while our analysis and the magnitude of our estimates are model dependent, the climate-change forcing, the mechanisms at play, and the relative changes in transit times should be more robust across models.

4 Conclusions and Discussion

We have introduced an idealized but computationally efficient framework to estimate the deep ocean's sequestration efficiency from existing climate-model output. Seafloor-to-surface TTDs were computed in a seasonally varying annually periodic flow representing the decadal climatology of the 2030s circulation of the ACCESS-ESM1.5 model for the SSP3-7.0 scenario. We repeated this analysis across a 40-member ensemble to assess the effect of climate variability, and then for the climatology of the 2090s circulation to assess the effect of climate change.

While sequestration efficiency is generally high on the abyssal plain, we found large geographical variations across basins, imparted by recognizable patterns of the ocean circulation. The most efficient sequestration can be found in isolated waters where transport back to the surface is dominated by slow diffusion. In contrast, abyssal waters that are swept into deep branches of the conveyor belt, which presents a relatively fast conduit back to the surface, provide the least efficient sequestration. Seafloor-to-surface TTDs generally skew strongly to the right, such that it generally takes about 30 % less time for half of the water to resurface compared to the mean reemergence time. The quantitative answers to the questions posed in this study are summarized below for the ACCESS-ESM1.5 model:

1. For abyssal basins that are swept by the conveyor belt, such as the Weddell Sea, the Bellingshausen, and the Australian-Antarctic Basins, it takes roughly 100 years for 10 % and up to 600 years for 50 % of the water to resurface (with a mean time of $\sim$ 1000 years). Waters in isolated abyssal plains take significantly longer, e.g., in the North Pacific Basins, where it can take up to 1300 years for 10 % and more than 2500 years for 50 % of the water to resurface ($>$ 3000 years on average).
2. Water sitting on the abyssal plain remains well sequestered on multi-centennial timescales, while the bulk of water on the continental shelf resurfaces in less than a century. The sequestration efficiency of the abyssal plain generally remains above 90 % after 100 years, above 80 % after 300 years, and above 30 % after 1000 years. The North Pacific Basins provide the most efficient sequestration, with more than 90 % of the water remaining below the surface after 1000 years. The Southwest Pacific Basin, north of the Pacific Antarctic Ridge also provides efficient sequestration ($>$ 80 % after 1000 years). In the Atlantic, the highest sequestration efficiency is found on the Canary Basin and the North American Basin, east and west of the Mid-Atlantic Ridge ($>$ 50 % after 1000 years).
3. Climate change generally skews the TTDs further to the right, increasing both reemergence times and sequestration efficiency, through its effect on the circulation. This effect is particularly pronounced for our 2090s circulation in the Weddell Sea where deep water formation is dramatically reduced, adding an average 1200 years of transit for seabed water to reemerge. In general, the seafloor-to-surface transit takes about 30 % more time, which is greater than internal climate-model variability at about 20 %.

Our work combines and highlights novel conceptual and computational methods that could benefit other modeling efforts. These methods include building monthly transport matrices from climate-model archives that accurately capture the ocean transport, efficient Newton–Krylov solvers for periodic solutions, efficient forward and backward time-stepping for estimating propagators and TTDs, and Anderson Acceleration for efficient spin up. We propose that applying some of these methods to a wide range of CMIP models could significantly improve our understanding of the ocean system.

Accurate estimates of ocean sequestration will be crucial for mCDR in the fight against climate change, for which the resources required are substantial (Smith et al., 2016; Sykes et al., 2020). It is therefore critical to plan mCDR projects in regions of the ocean where long-term storage is feasible. The reemergence timescales produced here are model-dependent but clearly highlight the higher sequestration potential of the North Pacific and other isolated abyssal plains. Applying our approach to other models will refine these estimates.

More broadly, our framework could straightforwardly be applied to other mCDR techniques, such as alkalinity enhancement, and beyond mCDR, potentially open up avenues for future research. This includes, for example, assessing the potential impacts of deep-sea mining on surface ecosystems through the seafloor-to-surface transit of trace metals (e.g., Drazen et al., 2020; Weaver et al., 2022).

Open Research

The ocean mass transport from resolved velocity fields used (the umo, vmo variables), grid metrics (areacello, volcello), and mixed layer depth variables (mlotst) are available on CMIP6 archives, e.g., at `https://esgf.nci.org.au/projects/esgfnci/`. For the unresolved Gent–McWilliams and submesoscale mass transport fields, which were not archived with CMIP6 for ACCESS-ESM1.5, we used output from CSIRO production archives of the corresponding MOM5 transport diagnostics of the ACCESS-ESM1.5 runs (using tx_trans_gm, ty_trans_gm, tx_trans_submeso, and ty_trans_submeso). The mean TTD ($\overline{\mathcal{G}^{\dagger}}$) and the mean sequestration efficiency ($\overline{\mathcal{E}}$) as plotted in the figures are available on Zenodo (Pasquier, 2025).

The code used in this work was written in Julia (Bezanson et al., 2017), Python (Van Rossum & Drake Jr, 1995), and MATLAB (The MathWorks Inc., 2022). The Python and Julia code used to preprocess CMIP6 output data is available at `https://github.com/TMIP-code/notebooks`. The Julia code used for building transport matrices from ocean model output (OceanTransportMatrixBuilder.jl; Pasquier, 2024) is available at `https://github.com/TMIP-code/OceanTransportMatrixBuilder.jl`. The Julia code for computing the adjoint boundary propagator and plotting the Figures (using Makie.jl; Danisch & Krumbiegel, 2021) of this manuscript is available at `https://github.com/TMIP-code/ACCESS-TMIP`. The MATLAB code for the Anderson Acceleration algorithm used (Khatiwala, 2023, 2024) for efficient spinup of the ACCESS-ESM1.5 water age is available at `https://github.com/briochemc/AndersonAcceleration/tree/ACCESS-ESM1-5`. The age was spun up by using the historical ACCESS-ESM1.5 model configuration (Ziehn et al., 2020) available at `https://github.com/ACCESS-NRI/access-esm1.5-configs` and using the infrastructure provided by ACCESS-NRI, which is enabled by the Australian Government's National Collaborative Research Infrastructure Strategy (NCRIS).

Acknowledgments

BP received funding from CSIRO's CarbonLock Future Science Platform. Computations were undertaken using Gadi, the supercomputer of the National Computational Infrastructure (NCI), which is supported by the Australian Government. MAC and TZ received funding from the Australian Government under the National Environmental Science Programme. DKH was supported by Australian Research Council Grant DE220100279. We thank Samar Khatiwala for helpful advice on setting up Anderson Acceleration. We thank

CSIRO and the ACCESS National Research Infrastructure (ACCESS-NRI) for developing ACCESS and making it freely available to researchers.

References

Arias, P., Bellouin, N., Coppola, E., Jones, R., Krinner, G., Marotzke, J., ... Zickfeld, K. (2021). Technical summary [Book Section]. In V. Masson-Delmotte et al. (Eds.), *Climate change 2021: The physical science basis. Contribution of working group I to the sixth assessment report of the intergovernmental panel on climate change* (pp. 33–144). Cambridge, United Kingdom and New York, NY, USA: Cambridge University Press. doi: 10.1017/9781009157896.002

Bardin, A., Primeau, F. W., & Lindsay, K. (2014). An offline implicit solver for simulating prebomb radiocarbon. *Ocean Modelling*, *73*, 45–58. doi: 10.1016/j.ocemod.2013.09.008

Bezanson, J., Edelman, A., Karpinski, S., & Shah, V. B. (2017). Julia: A Fresh Approach to Numerical Computing. *SIAM Review*, *59*(1), 65–98. doi: 10.1137/141000671

Chamberlain, M. A., Matear, R. J., Holzer, M., Bi, D., & Marsland, S. J. (2019). Transport matrices from standard ocean-model output and quantifying circulation response to climate change. *Ocean Modelling*, *135*, 1–13. doi: 10.1016/j.ocemod.2019.01.005

Danisch, S., & Krumbiegel, J. (2021). Makie.jl: Flexible high-performance data visualization for Julia. *Journal of Open Source Software*, *6*(65), 3349. doi: 10.21105/joss.03349

DeAngelo, J., Saenz, B. T., Arzeno-Soltero, I. B., Frieder, C. A., Long, M. C., Hamman, J., ... Davis, S. J. (2023). Economic and biophysical limits to seaweed farming for climate change mitigation. *Nature Plants*, *9*(1), 45–57. doi: 10.1038/s41477-022-01305-9

DeVries, T. (2022). The Ocean Carbon Cycle. *Annual Review of Environment and Resources*, *47*(1), 317–341. doi: 10.1146/annurev-environ-120920-111307

DeVries, T., & Holzer, M. (2019). Radiocarbon and helium isotope constraints on deep ocean ventilation and mantle-^{3}He sources. *Journal of Geophysical Research: Oceans*, *124*(5), 3036–3057. doi: 10.1029/2018JC014716

DeVries, T., & Primeau, F. W. (2011). Dynamically and Observationally Constrained Estimates of Water-Mass Distributions and Ages in the Global Ocean. *Journal of Physical Oceanography*, *41*(12), 2381–2401. doi: 10.1175/JPO-D-10-05011.1

DeVries, T., Primeau, F. W., & Deutsch, C. (2012). The sequestration efficiency of the biological pump. *Geophysical Research Letters*, *39*(13). doi: 10.1029/2012GL051963

Doney, S. C., Wolfe, W. H., McKee, D. C., & Fuhrman, J. G. (2024). The Science, Engineering, and Validation of Marine Carbon Dioxide Removal and Storage. *Annual Review of Marine Science*. doi: 10.1146/annurev-marine-040523-014702

Drazen, J. C., Smith, C. R., Gjerde, K. M., Haddock, S. H. D., Carter, G. S., Choy, C. A., … Yamamoto, H. (2020). Midwater ecosystems must be considered when evaluating environmental risks of deep-sea mining. *Proceedings of the National Academy of Sciences*, *117*(30), 17455–17460. doi: 10.1073/pnas.2011914117

Gattuso, J.-P., Williamson, P., Duarte, C. M., & Magnan, A. K. (2021). The Potential for Ocean-Based Climate Action: Negative Emissions Technologies and Beyond. *Frontiers in Climate*, *2*. doi: 10.3389/fclim.2020.575716

Gnanadesikan, A., Russell, J. L., & Zeng, F. (2007). How does ocean ventilation change under global warming? *Ocean Science*, *3*(1), 43–53. doi: 10.5194/os-3-43-2007

Griffies, S. M. (2012). Elements of the modular ocean model (mom) (2012 release with updates). *GFDL Ocean Group Tech. Rep.*(7), 620.

Haine, T. W. N., Griffies, S. M., Gebbie, G., & Jiang, W. (2024). A Review of Green's Function Methods for Tracer Timescales and Pathways in Ocean Models. *ESS Open Archive*. doi: 10.22541/essoar.172405906.63110239/v1

Haine, T. W. N., Zhang, H., Waugh, D. W., & Holzer, M. (2008). On transit-time distributions in unsteady circulation models. *Ocean Modelling*, *21*(1), 35–45. doi: 10.1016/j.ocemod.2007.11.004

Herzog, H. J. (2001). What Future for Carbon Capture and Sequestration? *Environmental Science & Technology - Columbus*, *35*(7), 148A.

Holzer, M., Chamberlain, M. A., & Matear, R. J. (2020). Climate-driven changes in the ocean's ventilation pathways and time scales diagnosed from transport matrices. *Journal of Geophysical Research: Oceans*, *125*(10), e2020JC016414. doi: 10.1029/2020JC016414

Holzer, M., DeVries, T., & de Lavergne, C. (2021). Diffusion controls the ventilation of a Pacific Shadow Zone above abyssal overturning. *Nature Communications*, *12*(1), 4348. doi: 10.1038/s41467-021-24648-x

Holzer, M., & Hall, T. M. (2000). Transit-Time and Tracer-Age Distributions in Geophysical Flows. *Journal of the Atmospheric Sciences*, *57*(21), 3539–3558. doi: 10.1175/1520-0469(2000)057⟨3539:TTATAD⟩2.0.CO;2

Holzer, M., & Primeau, F. W. (2006). The diffusive ocean conveyor. *Geophysical Research Letters*, *33*(14). doi: 10.1029/2006GL026232

Hurd, C. L., Law, C. S., Bach, L. T., Britton, D., Hovenden, M., Paine, E. R., ... Boyd, P. W. (2022). Forensic carbon accounting: Assessing the role of seaweeds for carbon sequestration. *Journal of Phycology*, *58*(3), 347–363. doi: 10.1111/jpy.13249

Khatiwala, S. (2023). Fast Spin-Up of Geochemical Tracers in Ocean Circulation and Climate Models. *Journal of Advances in Modeling Earth Systems*, *15*(2), e2022MS003447. doi: 10.1029/2022MS003447

Khatiwala, S. (2024). Efficient spin-up of Earth System Models using sequence acceleration. *Science Advances*, *10*(18), eadn2839. doi: 10.1126/sciadv.adn2839

Lenton, A., Matear, R. J., Keller, D. P., Scott, V., & Vaughan, N. E. (2018). Assessing carbon dioxide removal through global and regional ocean alkalinization under high and low emission pathways. *Earth System Dynamics*, *9*(2), 339–357. doi: 10.5194/esd-9-339-2018

Liu, Y., & Primeau, F. (2023). Surface-to-Interior Transport Timescales and Ventilation Patterns in a Time-Dependent Circulation Driven by Sustained Climate Warming. *Journal of Physical Oceanography*, *-1*(aop). doi: 10.1175/JPO-D-23-0113.1

Mannis, S., Waugh, D. W., Gnanadesikan, A., & Haine, T. W. N. (2024). Historical Trends in Ocean Heat, Carbon, Salinity, and Oxygen Simulations: Impact of a Changing Ocean Transport. *Journal of Geophysical Research: Oceans*, *129*(10), e2024JC021524. doi: 10.1029/2024JC021524

Nowicki, M., DeVries, T., & Siegel, D. A. (2024). The Influence of Air-Sea CO2 Disequilibrium on Carbon Sequestration by the Ocean's Biological Pump. *Global*

Biogeochemical Cycles, *38*(2), e2023GB007880. doi: 10.1029/2023GB007880

Oschlies, A., Pahlow, M., Yool, A., & Matear, R. J. (2010). Climate engineering by artificial ocean upwelling: Channelling the sorcerer's apprentice. *Geophysical Research Letters*, *37*(4). doi: 10.1029/2009GL041961

Pasquier, B. (2024). *OceanTransportMatrixBuilder.jl: A Julia package to build ocean transport matrices from CMIP model output.* Zenodo. doi: 10.5281/zenodo.14053323

Pasquier, B. (2025, May). *Data underlying the figures of The Sequestration Efficiency of the Deep Ocean, submitted to Geophysical Research Letters.* Zenodo. doi: 10.5281/zenodo.15321901

Pasquier, B., Holzer, M., & Chamberlain, M. A. (2024). The biological and preformed carbon pumps in perpetually slower and warmer oceans. *Biogeosciences*, *21*(14), 3373–3400. doi: 10.5194/bg-21-3373-2024

Pasquier, B., Holzer, M., Chamberlain, M. A., Matear, R. J., & Bindoff, N. L. (2024). Deoxygenation and Its Drivers Analyzed in Steady State for Perpetually Slower and Warmer Oceans. *Journal of Geophysical Research: Oceans*, *129*(9), e2024JC021043. doi: 10.1029/2024JC021043

Pessarrodona, A., Franco-Santos, R. M., Wright, L. S., Vanderklift, M. A., Howard, J., Pidgeon, E., … Filbee-Dexter, K. (2023). Carbon sequestration and climate change mitigation using macroalgae: A state of knowledge review. *Biological Reviews*, *98*(6), 1945–1971. doi: 10.1111/brv.12990

Primeau, F. W. (2005). Characterizing Transport between the Surface Mixed Layer and the Ocean Interior with a Forward and Adjoint Global Ocean Transport Model. *Journal of Physical Oceanography*, *35*(4), 545–564. doi: 10.1175/JPO2699.1

Primeau, F. W., & Holzer, M. (2006). The ocean's memory of the atmosphere: Residence-time and ventilation-rate distributions of water masses. *Journal of Physical Oceanography*, *36*(7), 1439–1456. doi: 10.1175/JPO2919.1

Riahi, K., Schaeffer, R., Arango, J., Calvin, K., Guivarch, C., Hasegawa, T., … van Vuuren, D. (2023). Mitigation pathways compatible with long-term goals. In P. Shukla et al. (Eds.), *IPCC, 2022: Climate Change 2022: Mitigation of Climate Change. Contribution of Working Group III to the Sixth Assessment Report of the Intergovernmental Panel on Climate Change* (chap. 3).

Cambridge University Press, Cambridge, UK and New York, NY, USA. doi: 10.1017/9781009157926.005

Riahi, K., van Vuuren, D. P., Kriegler, E., Edmonds, J., O'Neill, B. C., Fujimori, S., ... Tavoni, M. (2017). The Shared Socioeconomic Pathways and their energy, land use, and greenhouse gas emissions implications: An overview. *Global Environmental Change*, *42*, 153–168. doi: 10.1016/j.gloenvcha.2016.05.009

Ringrose, P. (2020). *How to Store CO2 Underground: Insights from early-mover CCS Projects*. Cham: Springer International Publishing. doi: 10.1007/978-3-030-33113-9

Romanou, A., Rind, D., Jonas, J., Miller, R., Kelley, M., Russell, G., ... Schmidt, G. A. (2023). Stochastic Bifurcation of the North Atlantic Circulation under a Midrange Future Climate Scenario with the NASA-GISS ModelE. *Journal of Climate*, *36*(18), 6141–6161. doi: 10.1175/JCLI-D-22-0536.1

Ross, F. W. R., Boyd, P. W., Filbee-Dexter, K., Watanabe, K., Ortega, A., Krause-Jensen, D., ... Macreadie, P. I. (2023). Potential role of seaweeds in climate change mitigation. *Science of The Total Environment*, *885*, 163699. doi: 10.1016/j.scitotenv.2023.163699

Siegel, D. A., DeVries, T., Doney, S. C., & Bell, T. (2021). Assessing the sequestration time scales of some ocean-based carbon dioxide reduction strategies. *Environmental Research Letters*, *16*(10), 104003. doi: 10.1088/1748-9326/ac0be0

Smith, P., Davis, S. J., Creutzig, F., Fuss, S., Minx, J., Gabrielle, B., ... Yongsung, C. (2016). Biophysical and economic limits to negative CO2 emissions. *Nature Climate Change*, *6*(1), 42–50. doi: 10.1038/nclimate2870

Sykes, A. J., Macleod, M., Eory, V., Rees, R. M., Payen, F., Myrgiotis, V., ... Smith, P. (2020). Characterising the biophysical, economic and social impacts of soil carbon sequestration as a greenhouse gas removal technology. *Global Change Biology*, *26*(3), 1085–1108. doi: 10.1111/gcb.14844

Talley, L. D. (2015). Closure of the Global Overturning Circulation Through the Indian, Pacific, and Southern Oceans: Schematics and Transports. *Oceanography*, *26*(1), 80–97. doi: 10.5670/oceanog.2013.07

The MathWorks Inc. (2022). *Matlab version: 9.13.0 (r2022b).* Natick, Massachusetts, United States: The MathWorks Inc. Retrieved from `https://www.mathworks.com`

Toggweiler, J. R., Druffel, E. R. M., Key, R. M., & Galbraith, E. D. (2019). Upwelling in the Ocean Basins North of the ACC: 1. On the Upwelling Exposed by the Surface Distribution of Δ^{14}C. *Journal of Geophysical Research: Oceans*, *124*(4), 2591–2608. doi: 10.1029/2018JC014794

Van Rossum, G., & Drake Jr, F. L. (1995). *Python tutorial.* Centrum voor Wiskunde en Informatica Amsterdam, The Netherlands.

Waugh, D. W., Hall, T. M., Mcneil, B. I., Key, R., & Matear, R. J. (2006). Anthropogenic CO2 in the oceans estimated using transit time distributions. *Tellus B: Chemical and Physical Meteorology*, *58*(5), 376–389. doi: 10.1111/j.1600-0889.2006.00222.x

Weaver, P. P. E., Aguzzi, J., Boschen-Rose, R. E., Colaço, A., de Stigter, H., Gollner, S., … Thomsen, L. (2022). Assessing plume impacts caused by polymetallic nodule mining vehicles. *Marine Policy*, *139*, 105011. doi: 10.1016/j.marpol.2022.105011

Wong, C. S., & Matear, R. J. (1998). Ocean disposal of CO2 in the North Pacific Ocean: Assessment of CO2 chemistry and circulation on storage and return to the atmosphere. *Waste Management*, *17*(5), 329–335. doi: 10.1016/S0956-053X(97)10049-6

Ziehn, T., Chamberlain, M. A., Law, R. M., Lenton, A., Bodman, R. W., Dix, M., … Srbinovsky, J. (2020). The Australian Earth System Model: ACCESS-ESM1.5. *Journal of Southern Hemisphere Earth Systems Science*, *70*(1), 193–214. doi: 10.1071/ES19035